DIFFRACTION TOMOGRAPHY ADAPTED TO TECHNICAL APPLICATIONS

Edgar Scherleitner, Bernhard G. Zagar

Institute for Measurement Technology, Johannes Kepler University of Linz, 4040 Linz, Austria

Abstract − An approach of a diffuse optical tomography system using NIR wavelengths will be presented to image heterogeneities in various kinds of turbid volumes, such as a wide range of biological substances, many translucent technical substances like plastics, foams and fluids.

A light intensity modulation technique is employed to achieve imaging of the absorption and additionally even the scattering properties of superior resolution than usual transillumination images of technical process monitoring. Since the understanding of photon migration in strongly scattering media has improved much lately, it is now possible to utilize inversion methods to solve for optical parameters out of a series of measurements. The discretized volume of the probe and the modeling of the light propagation by the diffusion equation give a linear system of equations, which is solved by singular value decomposition.

Keywords diffraction tomography nir

1. INTRODUCTION

Imaging and especially tomographic methods play a very important part in both, medical and technical examinations. To overcome the disadvantages of the widely used ionizing radiation, more and more research work is focused on diffraction tomography allowing to utilize low energy and thus harmless but still sufficiently penetrating light radiation. Visible and near infrared (NIR) wavelengths between 600 nm and 1000 nm are chosen for medical applications which comprise soft tissue testing for malignant masses as applicable to breast tissue scans for example. The primary intention of our examinations was to rather quickly obtain clear 2 dimensional images with respect to the absorption and scattering properties than to determine the exact values of these parameters

2. PRINCIPLE OF OPERATION

The principle of our system is very similar to that of the tomographic imaging methods that are more and more used for medical applications like non-invasive breast examinations etc. Amplitude-modulated light injected into the strongly scattering breast tissue causes randomly walking photons that macroscopically represent an exponentially damped spherical wave called Diffuse Photon Density Wave (DPDW) [1,5,8]. The propagation of these DPDWs depends on the intrinsic variations of the absorption and scattering properties thus the amplitude and phase differences of a received DPDW at another position of the breast contains information about the optical properties along the path that the photons have covered. Repeating some of those measurements at different positions one is capable to reconstruct a tomographic image of the breast in order to locate areas of deviating optical properties assumed to be malignant tissue. This method cannot only be used for medical examinations of tissue but similarly for all highly scattering substances in production control applications for example.

3. THEORY

Reconstructing the optical structure within a specimen from surface measurements only as described above constitutes mathematically an inverse problem, which can only be solved well if the propagation of the photons is appropriately modelled - this is usually called forward problem [1,4]. The theory behind this is rather extensive so that this chapter is split into two parts, the mathematical background of diffuse light propagation and the signal processing of the introduced system.

3.1. Mathematical background

The two most interesting optical properties of translucent substances are described by the absorption coefficient μ_a [cm^{-1}] and the diffusion coefficient D [cm^{2}s^{-1}], which is defined [1] by

$$D = \frac{v}{3\mu_s'} \qquad (1)$$

where v [cm s^{-1}] is the speed of light in the medium and μ_s' [cm^{-1}] is the reduced scattering coefficient, which is the reciprocal of the average distance for a photon to cover before its direction becomes random.

The propagation of light in sufficiently scattering and only weak absorbing media ($\mu_a \ll \mu_s'$) is very well comparable to a diffusion process thus the diffusion approximation to the Boltzmann transport equation is employed, which is

$$-\nabla \cdot D\nabla U(\mathbf{r},t) + v\mu_a U(\mathbf{r},t) + \frac{\partial U(\mathbf{r},t)}{\partial t} = vS(\mathbf{r},t) \quad (2)$$

where $\mathbf{r}$ is the vector of the currently observed position, $U(\mathbf{r},t)$ [cm^{-2}s^{-1}] is the photon fluence rate and $S(\mathbf{r},t)$ [cm^{-3}s^{-1}] is the isotropic source term (see also Fig. 1). With the following assumptions this partial differential equation can be solved by specifying the boundary conditions on some part of the surface of the regarded volume. These boundary conditions are both the source term $S(\mathbf{r}_s,t)$ fed into the volume by the primary source with a photon fluence rate $U(\mathbf{r}_s,t)$ depending on the current but varying position $\mathbf{r}_s$.

Examinations in the time domain like optical time domain reflectometry [9] have the disadvantage of much higher hardware costs since one needs very short pulse lasers (on the order of 10ps) combined with equally fast detectors, thus usually frequency domain techniques are chosen by modulating the primary source $S(\mathbf{r}_s,t)$ by a sine wave of frequency ω, by this modulation DPDWs are generated.

To obtain equations for the spatial variations of the absorption coefficient μ_a and the reduced scattering coefficient μ_s' the diffusion equation (2) must be adapted individually before it can be Fourier transformed [1-3]. For the absorption case the harmonic formulation of (2) gives

$$\left[\nabla^2 + k^2\right]U(\mathbf{r},\omega) = \frac{-v}{D}S(\mathbf{r},\omega) \quad (3)$$

where k is the complex wave number of the DPDW, the square of which is given by

$$k^2 = \frac{-v\mu_a + j\omega}{D} = 3\mu_s'\left(-\mu_a + j\frac{\omega}{v}\right). \quad (4)$$

After splitting up the absorption coefficient into a homogeneous and a spatially varying part as

$$\mu_a(\mathbf{r}) = \mu_a^0 + \delta\mu_a(\mathbf{r}) \quad (5)$$

one can rewrite (4) to yield

$$k^2 = k_0^2 + \delta k^2(\mathbf{r}) = \frac{-v\mu_a^0 + j\omega}{D} + \frac{-v}{D}\delta\mu_a(\mathbf{r}). \quad (6)$$

which finally gives a heterogeneous diffusion equation by substituting (6) into (3) and omitting ω in the notation for simplification

$$\left[\nabla^2 + k_0^2 + \delta k^2(\mathbf{r})\right]U(\mathbf{r}) = \frac{-v}{D}S(\mathbf{r}). \quad (7)$$
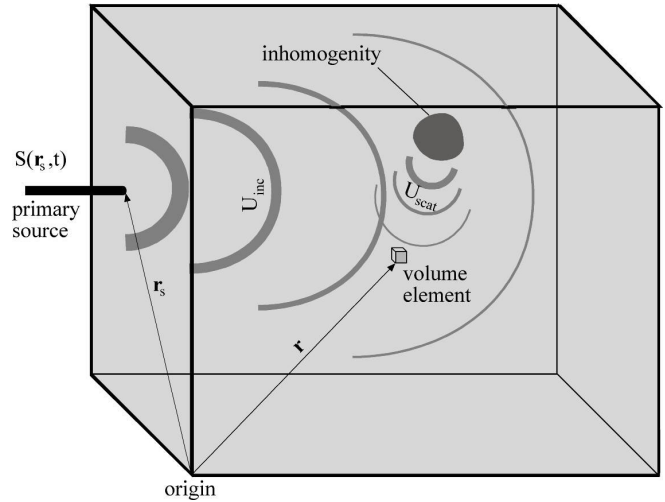

Fig. 1. A schematic of the propagation of DPDWs in a turbid medium with an embedded inhomogeneity. The incoming wave at each volume element at position $\mathbf{r}$ consists of both U_{inc} and U_{scat} due to the injected wave from the primary source and inhomogeneities respectively. The detector is placed on some place on the surface not specified.

To solve (7) one of the following two approximations are commonly used, the Born and the Rytov approximation [3,4]. Both split $U(\mathbf{r})$ into a homogeneous and a heterogeneous part:

Born:
$$U(\mathbf{r},\mathbf{r}_s) = U_{inc}(\mathbf{r},\mathbf{r}_s) + U_{scat}(\mathbf{r},\mathbf{r}_s) \quad (8)$$

Rytov:
$$U(\mathbf{r},\mathbf{r}_s) = \exp(\phi_{inc}(\mathbf{r},\mathbf{r}_s) + \phi_{scat}(\mathbf{r},\mathbf{r}_s))$$
$$= U_{inc}(\mathbf{r},\mathbf{r}_s) \cdot U_{scat}(\mathbf{r},\mathbf{r}_s) \quad (9)$$

where $\mathbf{r}_s$ indicates the primary source position. U_{inc} represents the incident part of U that would result from the source if no inhomogeneities were present. On the other hand U_{scat} is exclusively due to scattered light from inhomogeneities. The Rytov approximation is an exponential approach where U_{inc} and U_{scat} are introduced in the way shown in (9).

In our case the Rytov approximation was chosen to solve (7) because it has a better performance when spatial changes in the absorption coefficient exceed an amount of $0.1\,\text{cm}^{-1}$ [1,7]. Further explanations will merely refer to the Rytov approximation.

After discretizing the volume into voxels and the solution of (7) one is left with a linear system of equations of the form

$$\begin{pmatrix} \Phi_{scat}(\mathbf{r}_{s1},\mathbf{r}_{d1}) \\ \vdots \\ \Phi_{scat}(\mathbf{r}_{sm},\mathbf{r}_{dm}) \end{pmatrix} = \begin{pmatrix} w_{11} & \cdots & w_{1n} \\ \vdots & \ddots & \vdots \\ w_{m1} & \cdots & w_{mn} \end{pmatrix} \begin{pmatrix} \delta\mu_a(\mathbf{r}_1) \\ \vdots \\ \delta\mu_a(\mathbf{r}_n) \end{pmatrix} \quad (10)$$

where m is the number of different source-detector pairs, which is equal to the number of measurements and n, is the number of voxels. The complex elements w_{ij} of the matrix W are the so-called weight functions for each voxel as they indicate how much each voxel j influences the scattered wave at the detector position i during the current measurement. This system of equations can be solved by singular value decomposition [10], for example, to get a solution non-sensitive to singularities of the matrix W of the equation system.

In a similar but even more complex manner a system of equations for the scattering coefficient μ_s' is derived and solved. For a detailed derivation see [1,6].

3.1. Signal processing

The surface of the tested specimen is scanned step by step along a regular grid with a spacing on the order of some millimeters. At each position the amplitude and the phase differences between the source and the detector signal are recorded as a complex number Rec. After arranging all these measurements from different positions of the source-detector pair in a vector it can be fed into the implemented reconstruction algorithm.

Since these measured values represent the total field U (9) and not only the component due to inhomogeneities ϕ_{scat}, which is needed to solve (10) but also contains the homogeneous part ϕ_{inc} one has to eliminate ϕ_{inc} first. With (9) the signal Rec that is actually recorded at the location of the detector can be written as

$$Rec = C \cdot \exp(\Phi_{inc}) \exp(\Phi_{scat}) \qquad (11)$$

where C is a complex factor that summarizes all the changes in amplitude and phase caused by the system alone and which are not dependent on the observed specimen. Instead of determining C and ϕ_{inc} first a reference scheme [1] can be used alternatively by dividing two adjacent measurements and taking the natural logarithm as follows

$$\ln\left(\frac{Rec_1}{Rec_2}\right) = \ln\left(\frac{C \cdot \exp(\Phi_{inc}) \exp(\Phi_{scat1})}{C \cdot \exp(\Phi_{inc}) \exp(\Phi_{scat2})}\right) \qquad (12)$$

thus one obviously arrives at the difference $\Phi_{scat1} - \Phi_{scat2}$ of only the scattered parts of these two measured fields. After adapting the weight functions by performing the appropriate subtraction the algorithm solves for the desired $\delta\mu_a(\mathbf{r})$ and $\delta\mu_s'(\mathbf{r})$ for every voxel.

4. EXPERIMIMENTAL SETUP

4.1. Signal Processing Hardware

In a first step we designed our setup to scan slab geometries in order to examine various kinds of specimen that are either brought to a slab geometry in a proper small container, e.g. cotton-wool like fibers or fluids, or being
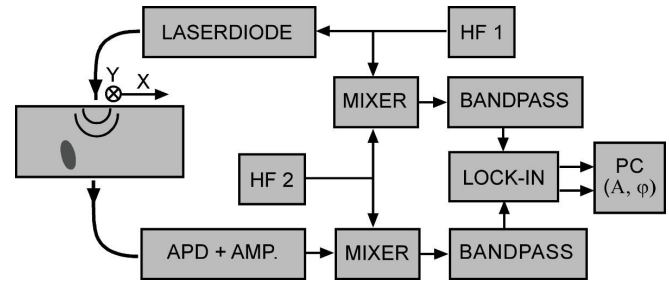

Fig. 2. Overview of the signal path in the system. The probe on the left hand side is penetrated by the photon density waves, the signal received by the APD is heterodyne demodulated and the amplitude and phase information is transferred to a PC for further processing.

already a slab geometry like plastic plates. Primarily it has been important for us to scan an area of the specimen to detect where an inhomogeneity is located without determining its exact depth. If one observes a production process it is important to find possible imperfections by monitoring both the absorption and scattering properties of produced material.

Fig. 2 shows a block-diagram of the tomographic system with the probe on the left hand side in a sectional view having one inhomogeneity.

A 50mW cw laser diode is used as an easy to modulate light source with a typical wavelength of 785nm. This wavelength was chosen to accommodate the spectral window of biological tissue but it is also sufficiently penetrating many materials of interest [5]. The light is coupled into and conducted to and from the specimen by standard optical fibers of 1mm core diameter. The fiber coupling was chosen to keep an appropriate distance between the circuit components of the system and the examined specimen if necessary. The specimen can easily be scanned in two dimensions due to the flexibility of the optical fibers to obtain measurements of all positions determined by the constraints of the subsequent signal processing algorithm. The movement of the fibers is managed by a PC controlled high precision 2-axes servomotor positioning system.

The high frequency signal source (HF1) provides the modulation signal for the laser diode with frequencies up to 1GHz. When the intensity-modulated light is applied to the source side of the specimen, as shown, diffuse photon density waves start to spread into the material. To receive the signal an avalanche diode attached to a low noise amplifier with a high cut-off frequency of 1GHz (APD+AMP.) is employed. A second signal source (HF2) is set to a frequency close to that of the modulation signal allowing heterodyne complex envelope demodulation. Two mixer circuits (MIXER) used to demodulate their respective input feed their output signals through two properly set band passes (BANDPASS) into a lock-in amplifier (LOCK-IN) to obtain both the phase shift and the ratio of the amplitudes between the source and the detector signal. These two signals are read into a PC via two AD-converters and the implemented algorithm performs the further signal processing as described before.
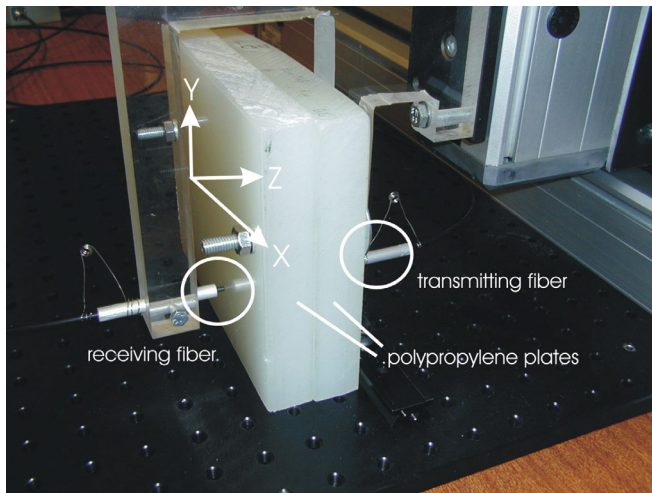
Fig. 3. The phantom A consisting of two plastic plates with an inhomogeneities placed in a hole between them is scanned by the source-detector pair located opposite of each other.
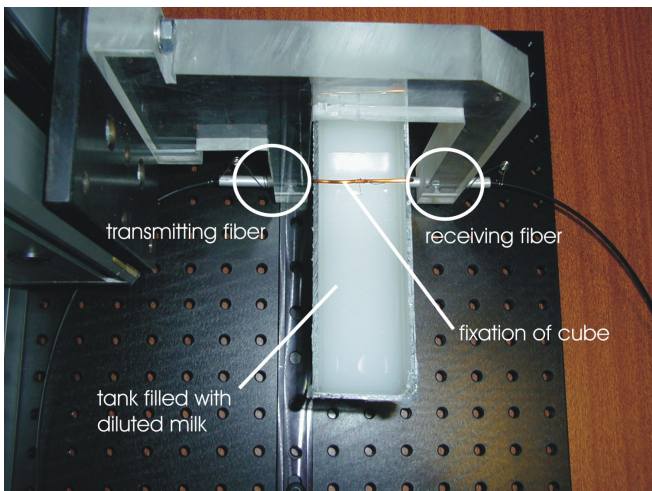

Fig. 4. Phantom B is a small Perspex tank filled with diluted milk in which an acrylic glass cube (not visible) hanging on a fine wire is embedded as an inhomogeneity.

4.2. Specimen Preparation

The first employed phantom (phantom A) is depicted in Fig. 3. It consists of two identical homogeneous poly-propylene plates with an expanse of 150x120mm and a thickness of 20mm, which are placed back-to-back and held together by two screws. In both plates a 5mm deep hole of 10mm diameter is drilled out at the exact opposite location, so that various inhomogeneities can easily be placed in the middle of the phantom. In order to achieve a semi-infinite geometry, that is necessary to satisfy the corresponding assumptions of the currently employed algorithm, the area that is investigated by the source-detector pair is more than 20mm smaller than the slab-phantom itself.

As a second phantom (phantom B) a small tank of the same external dimensions as the slab described above has been composed of Perspex plates of 2mm thickness. In this

container an acrylic glass cube with 10mm edge length is suspended from a fine wire as an inhomogeneity embedded in a mixture of water and condensed milk (250ml water, 15ml condensate milk with 17.5% fat). The transparent inhomogeneity can be considered to be weakly absorbing and much less scattering than the solution. A top view of phantom B can be seen in Fig. 4.

5. RESULTS AND DISCUSSION

The scanned area is extended 50mm in horizontal (X) and 45mm in vertical (Y) direction. Measurements of amplitude and phase differences are taken on a grid with 5mm pitch whereas every other position is used to obtain reference values which results in 110 measurements altogether. The volumes of the two phantoms are equally discretized into unitary cubic voxels with an edge length of 5mm. When the superficial layers of voxels is excluded on each side of the slab in order to go with the assumption of randomly directed light, the number of voxels accounts for 770.

5.1. Measurement A

The borehole of phantom A is filled with black foam which can be considered to be an ideal absorber whose center is located at the position X=3cm, Y=3cm and Z=2cm. The images being indicative of the absorption coefficient in the cross sections at depths 1.5cm, 2.0cm and 2.5cm are shown in Fig. 5.

The reconstructed X-Y position is very accurate and the size of the white area, which indicates absolute absorption, matches exactly the size of the cross-section of cylinder in phantom A.

The very small differences seen in these three cross-sectioned views seem to be quite what would be expected but as a matter of fact the slices closer to the surface look very similar too and are thus not depicted here. This lack in resolution in depth (Z-direction) is a consequence of the fixed source-detector alignment opposite of each other and could be improved by taking measurements at oblique source-detector positions as well.

5.2. Measurement B

The acrylic glass cube is positioned at X=3cm, Y=3cm and Z=2cm and cannot be seen in the shining-through light. Fig. 6 shows the scattering variations that are clearly resolved, again without a depth resolution as explained above. The mapping of the absorption properties in Fig. 7 also shows a variation because the acrylic glass cube acts like a kind of absorber for the propagating DPDW since multiple reflections inside the cube end up in a partial turning back of the photons. In addition the Rytov approximation makes the assumption that the scattered field is only slowly varying which is not the truth in this case resulting in the observed ringing artefacts.
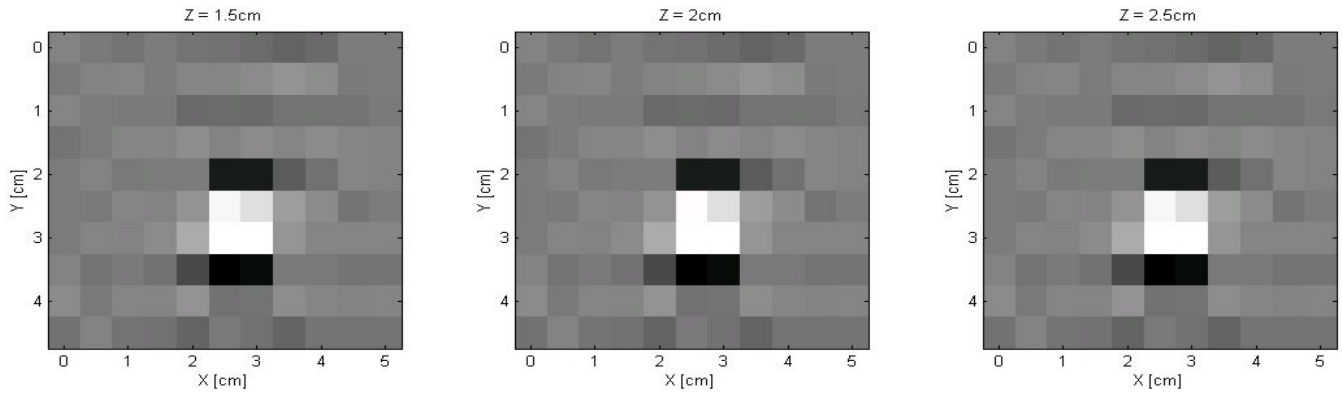
Fig. 5. Mapping of absorption coefficient of phantom A containing a black foam cylinder with a radius of 0.5cm and a length of 1cm as an absorbing inhomogeneity at the position X=3cm, Y=3cm and Z=2cm. The figure shows three different cross-sections at depths of 1.5, 2.0 and 2.5cm. Brighter areas have a higher absorption than darker ones.
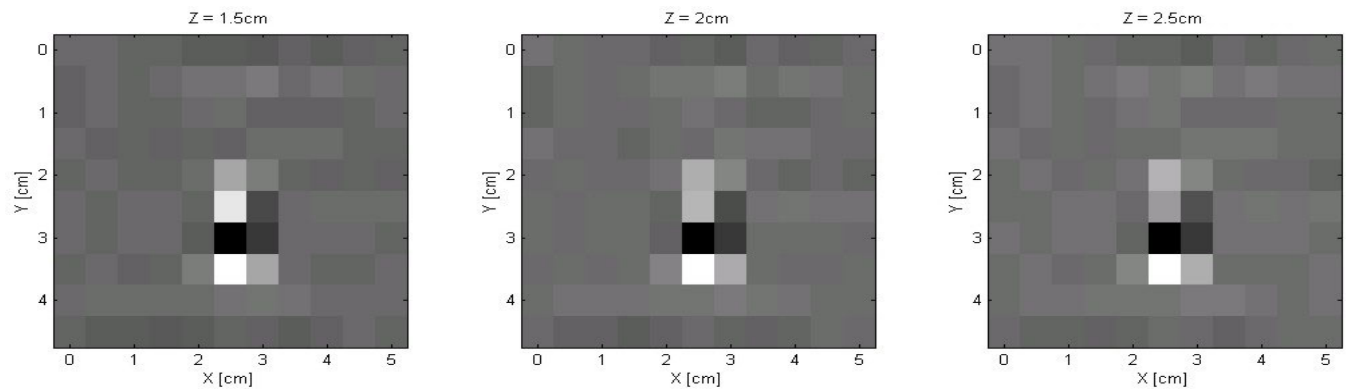

Fig. 6. Mapping of scattering coefficient of Phantom B. The inhomogeneity, an acrylic glass cube, is positioned at X=3cm, Y=3cm and Z=2cm. The figure shows three different cross-sections at depths of 1.5, 2.0 and 2.5cm.
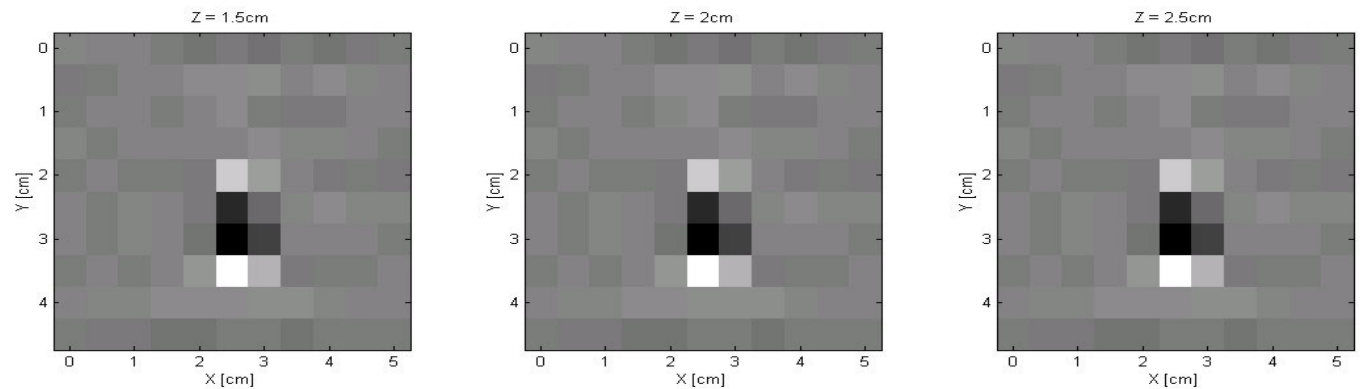

Fig. 7. Mapping of scattering coefficient of Phantom B. The inhomogeneity, an acrylic glass cube, is positioned at X=3cm, Y=3cm and Z=2cm. The figure shows three different cross-sections at depths of 1.5, 2.0 and 2.5cm.

6. CONCLUSIONS AND FUTURE WORK

In this paper we show that accurate cross sectional views can be achieved by evaluating the Rytov approximation of the diffusion equation. Major improvements in depth resolution are expected by choosing not only face-to-face source-detector positions but also sloping positions in order to obtain side views of possible inhomogeneities as well.

It is expected that an increase in image quality will be accomplished by implementing appropriate boundary conditions for the examined specimen geometries such as

Dirichlet boundary conditions by using an image source to set $U=0$ on the surface.

REFERENCES

[1]   M. A. O'Leary, "Imaging with diffuse photon density waves", *doc. diss.* M. A. O'Leary , Univ. of Pennsylvania, 1996

[2]   M. S. Patterson, B. Chance, B. C. Wilson, "Time resolved reflectance and transmittance for the non–invasive measurement of tissue optical properties*", Applied Optics,* vol. 28, no. 12, 1989

[3] A. C. Kak, M. Slany, "Principles of Computerized Tomographic Imaging", *IEEE Press,* 1988

[4] R. Gaudette, "Constrained Reconstruction Techniques for Diffuse Optical Tomography", *doc. diss.* R. Gaudette (2000), Athinoula A. Martinos Center for Biomedical Imaging

[5] V. V. Tuchin, " Light Scattering study of tissues", *Uspekhi Fizicheskikh Nauk*, 1997

[6] V. Ntziachristos, A. H. Hielscher, A. G. Yodh, B. Chance, "Diffuse Optical Tomography of Highly Heterogeneous Media*", IEEE Transaction on Medical Imaging*, vol. 20, no. 6, 2001

[7] R. J. Gaudette, D. H. Brooks, C. A. DiMarzio, M. E. Kilmer, E. L. Miller, et al., "A Comparison study of linear reconstruction techniques for diffuse optical tomographic imaging of absorption coefficient", *Phys. Med. Biol*. 45, pp. 1051-1070, 2000

[8] M. A. O'Leary, D. A. Boas, B. Chance, A. G. Yodh, "Experimental images of heterogeneous turbid media by frequency-domain diffusion-photon tomography", *Optics Letters*, vol. 20, no. 5, 1995

[9] S. Willmann, "Scattered Light Spectroscopy of Photon Density Waves", "Streulichtspektroskopie mit Hilfe von Photonendichtewellen", doc. diss. S. Willmann, Univ. of Düsseldorf, 1999

[10] W. H. Press, S. A. Teulkolsky, W. T. Vetterling, B. P. Flannery, "Numerical Recipes in C++", *Cambridge University Press*, 2002

Authors: Edgar Scherleitner, Prof. Dr. Bernhard G. Zagar, Institute for Measurement Technology, University of Linz, Altenbergerstrasse 69, 4040 Linz, Austria, +43-70-2468-9208, fax +43-70-2468-9233, edgar.scherleitner@jku.at, bernhard.zagar@jku.at .